Simulation studies of a recorder in three dimensions

N. Giordano[a)]
Department of Physics, Purdue University, West Lafayette, Indiana 47907

(Received 23 July 2013; revised 25 November 2013; accepted 12 December 2013)

The aeroacoustics of a recorder are explored using a direct numerical simulation based on the Navier–Stokes equations in three dimensions. The qualitative behavior is studied using spatial maps of the air pressure and velocity to give a detailed picture of jet dynamics and vortex shedding near the labium. In certain cases, subtle but perhaps important differences in the motion of the air jet near the edge of the channel as compared to the channel center are observed. These differences may be important when analyzing experimental visualizations of jet motion. The quantitative behavior is studied through analysis of the spectrum of the sound pressure outside the instrument. The effect of chamfers and of changes in the position of the labium relative to the channel on the tonal properties are explored and found to be especially important in the attack portion of the tone. Changes in the spectrum as a result of variations in the blowing speed are also investigated as well as the behavior of the spectrum when the dominant spectral component switches from the fundamental to the second harmonic mode of the resonator tube.
 [http://dx.doi.org/10.1121/1.4861249]

PACS number(s): 43.75.Qr, 43.75.Zz, 43.75.Bc [TRM] Pages: 906–916

I. INTRODUCTION

In a recent paper,[1] the author presented results of a study of a two dimensional model of the recorder using numerical solutions of the Navier–Stokes equations. In this paper, the extension of that work to a fully three dimensional model of the recorder is described. One goal is to use Navier–Stokes based modeling to elucidate how the tonal properties of the recorder and of the closely related case of a flue organ pipe depend on the detailed geometry of the channel and labium. We also explore the transition to higher notes as the blowing speed is increased.

A broader goal of our work is to use Navier–Stokes based modeling of a relatively simple wind instrument (the recorder) to explore how specific features of the instrument affect the quantitative tonal properties. In this way, modeling may lead to changes in instrument design as well as ways to extract more detailed information from experimental studies.

II. BACKGROUND

The application of the Navier–Stokes equations to model the behavior of wind instruments such as the recorder is extremely challenging as the numerical solution of these equations requires considerable computer power to explore regimes of musical interest. Many of the previous applications of the Navier–Stokes equations in this area have focused on the family of instruments that includes recorders and flue organ pipes[1–16] and have yielded intriguing pictures of the fluid motion that leads to sound production. However, because of limitations on computing power, much of this work has been restricted to simplified geometries (e.g., instruments in two dimensions) and to short time scales (typically 10 or 20 ms). While great progress has been made, much remains to be done. In this paper, we describe in detail results of a Navier–Stokes based study of a fully three dimensional recorder. We have recently given preliminary reports on some of this work in Refs.16 and 17; in this paper, we give a full description of the results.

A. Model geometry

The basic geometry we have modeled is shown in Fig. 1(a). Air enters a straight, narrow channel of height h from the left and upon exit from the channel strikes the labium. The labium is a sharp triangular edge positioned a distance W beyond the exit of the jet. The labium is located above a long "tube" of length L, height d, and width [in the direction perpendicular to the plane of Fig. 1(a)] d. The far right end of the tube in Fig. 1(a) is open to the region surrounding the instrument.

For all the results shown in this paper, we have used [see Fig. 1(a)] $h = 1.0$ mm, $L_c = 8.0$ mm, $L = 195$ mm, and $d = 10.0$ mm, making this roughly comparable to a sopranino recorder. For this value of L, the expected value for the fundamental frequency (including end corrections) is about 1400 Hz. The labium distance W was 4.0 mm, giving a ratio $W/h = 4$, which is typical for the instrument.[18] The labium angle was $\theta \approx 12^\circ$ (corresponding to $\tan\theta = 0.2$).

The recorder drawn in Fig. 1(a) has a straight channel with the bottom edge of the labium aligned with the center of the channel. We also studied the behavior with the labium aligned with the bottom of the channel (as is often found in real instruments) and with chamfers added to the end of the channel. A chamfer is a beveled edge at the exit of the channel [Fig. 1(b)]. We have investigated the behavior with one chamfer (on the bottom edge of the channel) and two chamfers [on both the bottom and top edges, as in Fig. 1(b)]. In all cases, the chamfers made a 45° angle with the exit plane of the channel and extended 0.4 mm on the sides parallel and perpendicular to the channel.

a)Author to whom correspondence should be addressed. Current address: Department of Physics and College of Sciences and Mathematics, Auburn University, Auburn, AL 36849; njg0003@auburn.edu

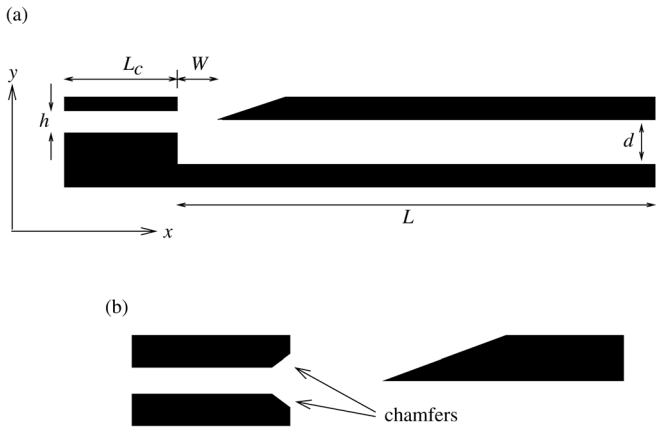

FIG. 1. (a) Cross section of the three dimensional recorder studied in this work (not to scale). The z direction is perpendicular to the plane of the drawing. (b) Exploded view of the flue region, showing a channel with chamfers on the top and bottom surfaces.

For our simulations, the instrument was enclosed in a (virtual) room that was typically 0.2 m wide (along x), and 0.06 m tall (along y), and 0.06 m wide (along z); a few simulations with larger regions (which required more computer time) gave similar results for the spatial variations of the density and air velocity and for the sound spectra. There was open space on all sides of the instrument, with most of this space being above and to the right in Fig. 1(a), to allow ample room for vortex motion above the labium.

B. Numerical method

The numerical method we have employed is the same as that used in our two dimensional studies;[1] here we give only a few details pertaining to the three dimensional case.

We denote the components of the velocity along x, y, and z [see Fig. 1(a)] as u, v, and w respectively, the density as ρ, the speed of sound by c, and the kinematic viscosity by ν. The Navier–Stokes equations for air in the limit that applies to the air flow in a recorder (a viscous, compressible fluid at low Mach number, taking the ideal gas equation of state and assuming adiabatic conditions) can be written as[2,19]

$$\frac{\partial \rho}{\partial t} + \frac{\partial(\rho u)}{\partial x} + \frac{\partial(\rho v)}{\partial y} + \frac{\partial(\rho w)}{\partial z} = 0, \tag{1}$$

$$\frac{\partial u}{\partial t} + u\frac{\partial u}{\partial x} + v\frac{\partial u}{\partial y} + w\frac{\partial u}{\partial z} + \frac{c^2}{\rho}\frac{\partial \rho}{\partial x} - \nu \nabla^2 u = 0, \tag{2}$$

$$\frac{\partial v}{\partial t} + u\frac{\partial v}{\partial x} + v\frac{\partial v}{\partial y} + w\frac{\partial v}{\partial z} + \frac{c^2}{\rho}\frac{\partial \rho}{\partial y} - \nu \nabla^2 v = 0, \tag{3}$$

$$\frac{\partial w}{\partial t} + u\frac{\partial w}{\partial x} + v\frac{\partial w}{\partial y} + w\frac{\partial w}{\partial z} + \frac{c^2}{\rho}\frac{\partial \rho}{\partial z} - \nu \nabla^2 w = 0\,. \tag{4}$$

Variations in pressure from the background value (denoted $p = P - P_0$, where P_0 is the pressure when the blowing speed is zero) are related to the corresponding variations in the density ($\rho - \rho_0$, where ρ_0 is the density when the blowing speed is zero) by

$$p = P - P_0 = c^2(\rho - \rho_0). \tag{5}$$

To solve Eqs. (1)–(4), we used the explicit MacCormack method,[20] a finite difference, predictor-corrector algorithm that is second order accurate.[19] It is well known that long-time integrations of the Navier–Stokes equations can lead to numerical instabilities.[19] To suppress these instabilities, we added "artificial" viscosity following the approach described by Jameson and coworkers[21] in which additional viscosity-like terms are inserted into the Navier–Stokes equations for ρ, u, v, and w. The precise form of these terms is described in Refs. 1 and 21. The added terms bear a formal resemblance to the viscosity terms in Eqs. (2)–(4) and serve to damp rapid variations that occur on very short spatial scales. The key point is that this damping depends on the spatial scale, so that instabilities at very small length scales are suppressed, while keeping the effective viscosity at the scales of acoustic interest equal to the real viscosity of air.

C. Computational considerations

The computations were performed using a rectilinear grid with space discretized in units of Δx along x, Δy along y, and Δz along z, and time discretized in units of Δt. The grid spacing was different along the three coordinate directions and was also nonuniform with smaller spacings in and near the channel and labium, and larger spacings far from the recorder. The smallest spacings (used near the channel and labium, and throughout the tube) were $\Delta y = 0.1$ mm, $\Delta x = 0.2$ mm, and $\Delta z = 1$ mm, and the largest spacings used far from the recorder were less than 2 mm. The total number of grid points was typically 3×10^7. The grid spacing was thus always at least a factor of 10 smaller than the smallest feature on the recorder in any particular direction and was also much smaller than the wavelength at the highest frequencies of interest. The time step required for numerical stability was then set by the Courant condition[19] as $\Delta t < F\Delta y/c$ where F is a numerical factor of order 0.5. Because of our use of a rectilinear grid, the upper (sloped) surface of the labium was actually a "staircase." However, we do not believe that this had a significant effect on the results as calculations with both larger and smaller grid spacings gave similar results as did calculations with different sizes for the region enclosing the recorder.

The following boundary conditions were used at the edges of the simulation region and on the surfaces of the recorder: (1) Non-slip conditions; i.e., the component of the velocity parallel to each surface was zero, and (2) the perpendicular component of the velocity, $v_\perp$, was related to the variation of the pressure at the surface through a mechanical impedance Z where[22]

$$p = P - P_0 = Z v_\perp\,. \tag{6}$$

Following Refs. 22 and 23, Z was given a frequency dependence

$$Z = Z_0 + j\omega Z_1, \tag{7}$$

where $j = \sqrt{-1}$. The imaginary part of Z was much smaller than the real part, yielding reflection of sound at the

boundaries with a small amount of damping. The form for the impedance in Eq. (7) is expressed in the frequency domain, whereas our finite difference algorithm is based in the time domain. The implementation of Eq. (7) in the time domain was accomplished using the approach described by Botteldooren.[22,23] We assumed acoustically "hard" surfaces with $Z_0 = 10^6\,\mathrm{kg/s}$ for the recorder and boundaries (values obtained from the data in Ref. 24) with weak absorption $Z_1 = 1\,\mathrm{kg/m^2}$ for the surfaces of the recorder and somewhat stronger absorption $Z_1 = 10\,\mathrm{kg/m^2}$ at the boundaries of the computational region (the virtual room).

The model recorder in Fig. 1(a) was located in a closed computational region with no in-flow or out-flow. The recorder was excited by imposing a fluid velocity in the left half of the channel in Fig. 1(a). This imposed velocity was parallel to the channel ($v = w = 0$) with a magnitude of u that varied with y and z within the channel so as to match the solution for Poiseuille flow. A corresponding density gradient was also imposed in this region as derived from Eq. (2). The imposed velocity and the corresponding density gradient were increased linearly from zero at $t = 0$ to their final values at $t = 5$ ms. This is approximately seven periods of the fundamental frequency of oscillation of the instrument. This method of "blowing" the instrument was intended to give a general flow pattern like that found in real playing, with a gradual build-up starting from no net flow, to a situation with a constant flow rate out of the channel. There was then a net circulation out of the region near the labium and the far end of the recorder back to the inlet of the channel. The simulations were run for typically 0.05–0.1 s with the blowing speed ramped up from zero at $t = 0$ to a constant value that was maintained for the duration of the simulation. Steady state was usually reached after about 25 ms.

The computations were carried out on a high performance compute cluster at the Rosen Center for Advanced Computing at Purdue University. Specifically, we employed a system in which either 16 or 48 cores shared a common memory. Given the nature of the algorithm, this resulted in a compute time compared to that found with a single processor core that was reduced by a factor of approximately $0.9 \times N$ where N was the number of cores. Typically 1 ms of sound could be calculated in about 2 h of real time.

III. QUALITATIVE RESULTS: SPATIOTEMPORAL BEHAVIOR OF THE DENSITY AND VELOCITY

Figure 2 shows spatial maps of the air density in and around the instrument. Because the sound pressure is proportional to the deviation of the density from the average (background) density, these are also maps of the sound pressure. The entrance to the channel is on the left, and it plus the body of the tube are outlined in black. These images were recorded at three instants during the course of one period of an oscillation and show a standing wave inside the tube. In Fig. 2(a), the density at the middle of the tube is large in magnitude and negative with the density smoothly approaching the background value at the ends of the tube. The image in Fig. 2(b) was recorded half a period later, and the density at the middle of the tube is now large and positive. The image in Fig. 2(c) was recorded approximately another half period later and is essentially identical to the image in Fig. 2(a).

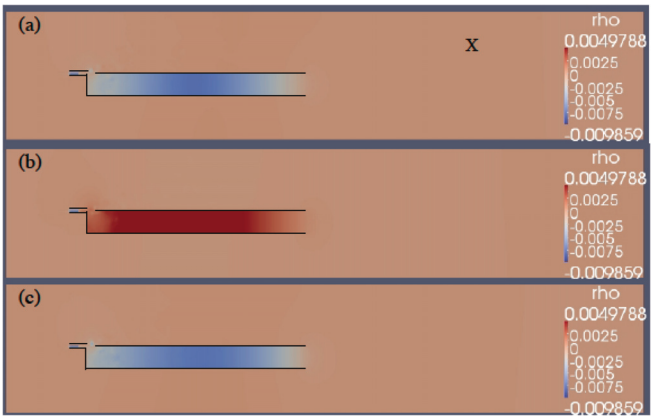

FIG. 2. Images of the density on the $x - y$ plane that cuts vertically through the center of the recorder. These images show the density at three times during the course of one oscillation cycle. The dark blue color corresponds to a low density and dark red to a high density. These figures show approximately the entire simulation region, with the recorder walls outlined in black. The "X" in (a) is the location at which the results for the sound pressure as a function of time presented in the following text were recorded. For this simulation, the blowing speed at the center of the channel was $u_0 = 25\,\mathrm{m/s}$, and the images were recorded after reaching steady state. Here and in Fig. 3 the labium was aligned with the center of the channel and the channel had straight walls (no chamfers), although on this scale the behavior was essentially identical for the different channel and labium geometries that were studied. The numerical scales on the right translate the color code to variations of the density as measured in $\mathrm{kg/m^3}$.

Figure 3 shows images of the air jet during the course of one oscillation obtained in the same simulation as the one that yielded the density maps in Fig. 2. The images in Fig. 3 span approximately one period of the motion, so images Figs. 3(a) and 3(h) are nearly identical. The air jet is seen to oscillate above and below the tip of the labium, as expected, and the behavior is qualitatively similar to that observed in experimental studies of recorders and flue organ pipes (see, e.g., Ref. 25). Note that the behavior seen here in three dimensions is different from that found in two dimensions,[1] where the jet never moved below the labium. This is due to an important difference in the way vortices and eddies change shape and dissipate energy in three as compared to two dimensions as discussed in Ref. 14. (See also, e.g., Ref. 26.)

IV. EFFECT OF CHANNEL AND LABIUM GEOMETRIES ON TONAL PROPERTIES

It is well known that the tonal properties of a flue pipe depends on its geometry. One important geometrical factor is the ratio W/h, where W is the distance from the exit of the channel to the labium and h is the height of the channel [Fig. 1(a)]. For our work, we have kept that ratio at $W/h = 4$, the value found for most recorders (but not organ pipes), and have investigated how changes in the shape of the exit portion of the channel and the position of the bottom edge of the labium affect the resulting tone. In the next two subsections, we consider how these variations in the geometry affect the early (attack) part of the tone and the tone at long times

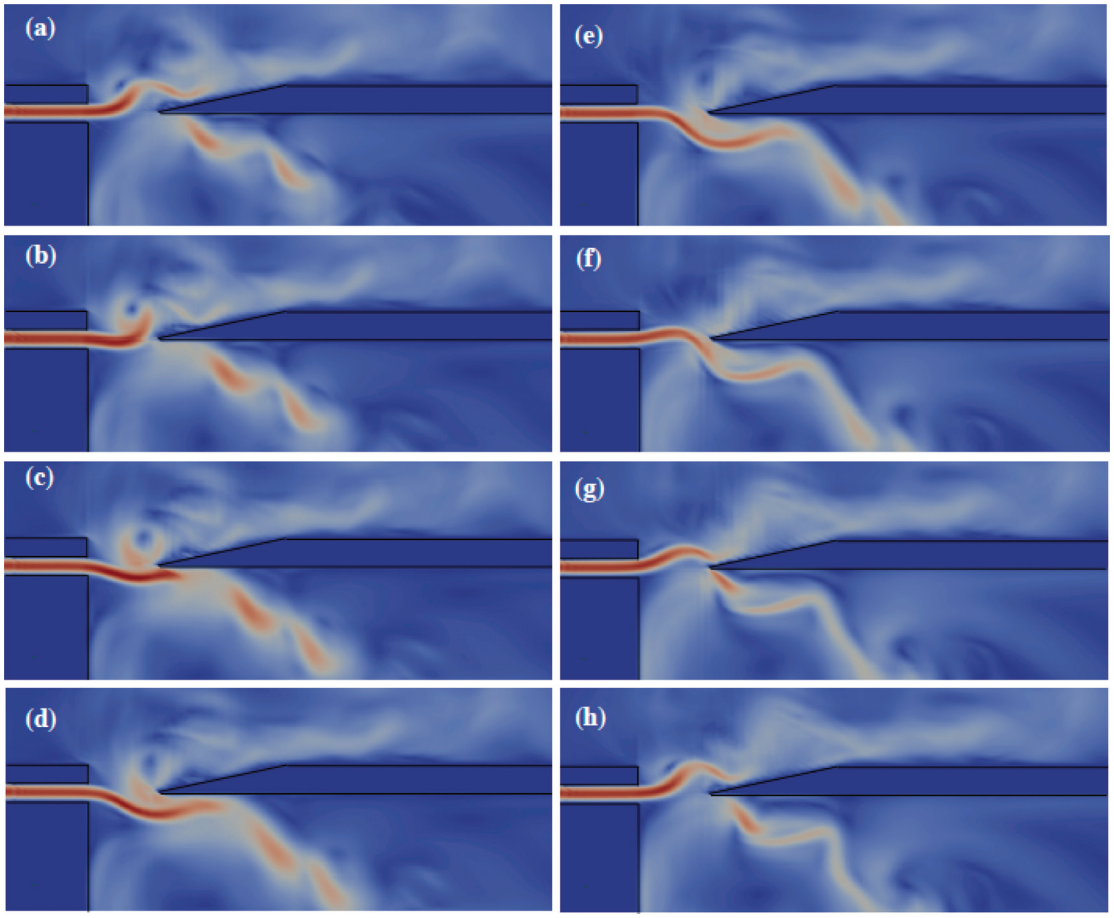

FIG. 3. Images of the air speed near the exit of the channel and labium on the $x-y$ plane that cuts vertically through the center of the recorder, recorded at 0.1 ms intervals. The images (a)—(h) span approximately one oscillation cycle. The dark red color corresponds to the highest speed and dark blue to the lowest speed. Edges of the channel, labium, and other surfaces of the recorder are outlined with black lines. For this simulation the blowing speed at the center of the channel was $u_0 = 25\,\mathrm{m/s}$.

(steady state). In a very interesting study, Segoufin and coworkers[27] have explored experimentally the effect of chamfers for the value of $W/h = 4$ (the value used in our modeling) for what they term long and short channels. Their long channels were chosen so as to exhibit Poiseuille flow; because our modeling imposes Poiseuille flow in the channel, we will be comparing with the long channel results of Segoufin *et al*.

A. Behavior of the attack portion of the tone

Typical results for the sound pressure as a function of time are shown in Fig. 4. These results were obtained from the density variations at a point outside the tube (Fig. 2) along with Eq. (5). Here and in the remainder of this paper, we chose to analyze spectra obtained at a point outside the tube so as to avoid complications due to the effect of the standing wave inside the tube on the overall amplitude of the sound pressure. For the blowing speed in Fig. 4, the sound pressure level inside the tube was approximately 130 dB, a typical value for real recorders.

As noted in the preceding text, in this simulation and in all the other results reported in this paper, the blowing speed was increased linearly with time from zero at $t = 0$ to a final steady value at $t = 5$ ms. Even though the final value of the blowing speed was established at $t = 5$ ms, the sound amplitude at that time was very small, as the sound pressure took much longer to reach steady state. In this case, steady state was reached around $t = 25$ or 30 ms. The oscillations seen here between 30 and 50 ms were maintained for the duration of the simulation, which was as long as 150 ms in some cases.

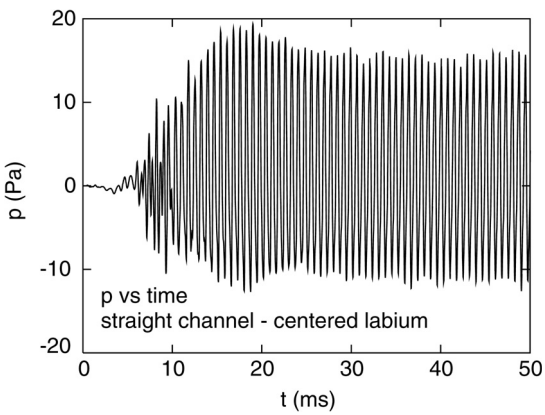

FIG. 4. Sound pressure $p = P - P_0$ as a function of time at a typical point outside the tube, approximately the location of the "X" in Fig. 2(a). Here $u = 30$ at the center of the channel. The channel was straight with no chamfers, and the labium was aligned with the center of the channel.

The behavior of the sound pressure in Fig. 4 in the steady state regime ($t > 25$ ms) was dominated by the component at the fundamental frequency of about 1380 Hz (see following text). However, at early times, before steady state was reached, the spectral composition was more complex. This is visible by eye from Fig. 5(a), which shows an expanded view of the pressure as a function of time during the attack portion of the tone. Figures 5(b)–5(d) show how the attack portion of the tone changes when the geometry of the channel and labium are varied. Part (a) of this figure shows the behavior for a straight channel with the labium edge aligned with the center of the channel [the geometry drawn in Fig. 1(a)]. Figure 5(b) shows the behavior with the labium lowered so that it is aligned with the bottom of the channel. Parts (c) and (d) of the figure show results for the labium aligned with the center of the channel and with one chamfer added to the bottom of the channel [part (c)] and with chamfers added to the top and bottom edges of the channel [part (d)]. These relatively small changes to the geometry are seen to produce large changes in the overall level of the tone, in the rise time of the sound pressure, and in the spectral composition of the attack portion of the tone.

Results of an analysis of the attack spectrum are shown in Fig. 6. Here we have computed spectra using Fourier transforms during the intervals 5–10, 10–15, and 20–25 ms. The simplest behavior is found with the channel with two chamfers, Fig. 6(d). Here the spectra during all three intervals are dominated by a fundamental component around $f_1 \approx 1400$ Hz with a second weaker component indicated by the arrows with a frequency $f_2 \approx 2 \times f_1$. This component at f_2 thus appears to be a second harmonic. A peak consistent with being a third harmonic is also visible. The behavior for the straight channel and centered labium [Fig. 6(a)] is quite different. Here the frequency f_2 of the second peak (again indicated by the arrows) during the 5–10 ms period is about 500 Hz lower than $2 \times f_1$. This second peak is also about equal in power as compared to the component at the fundamental. The second peak then shifts to a higher frequency, consistent with $2 \times f_1$, in the period 10–15 ms and thereafter. This means that the attack portion of this tone is distinctly inharmonic with a spectral composition that varies during the attack.

The behavior for a channel with one chamfer [Fig. 6(c)] is qualitatively similar to that found with a straight channel, but the inharmonic component during 5–10 ms is considerably smaller. With the labium aligned with the bottom of the channel and no chamfers [Fig. 6(b)], the fundamental component at early times is weaker than the inharmonic component, again exhibiting a complex attack behavior.

The time dependence of the spectral components at frequencies f_1 and f_2 during the attack is shown in Fig. 7. Here

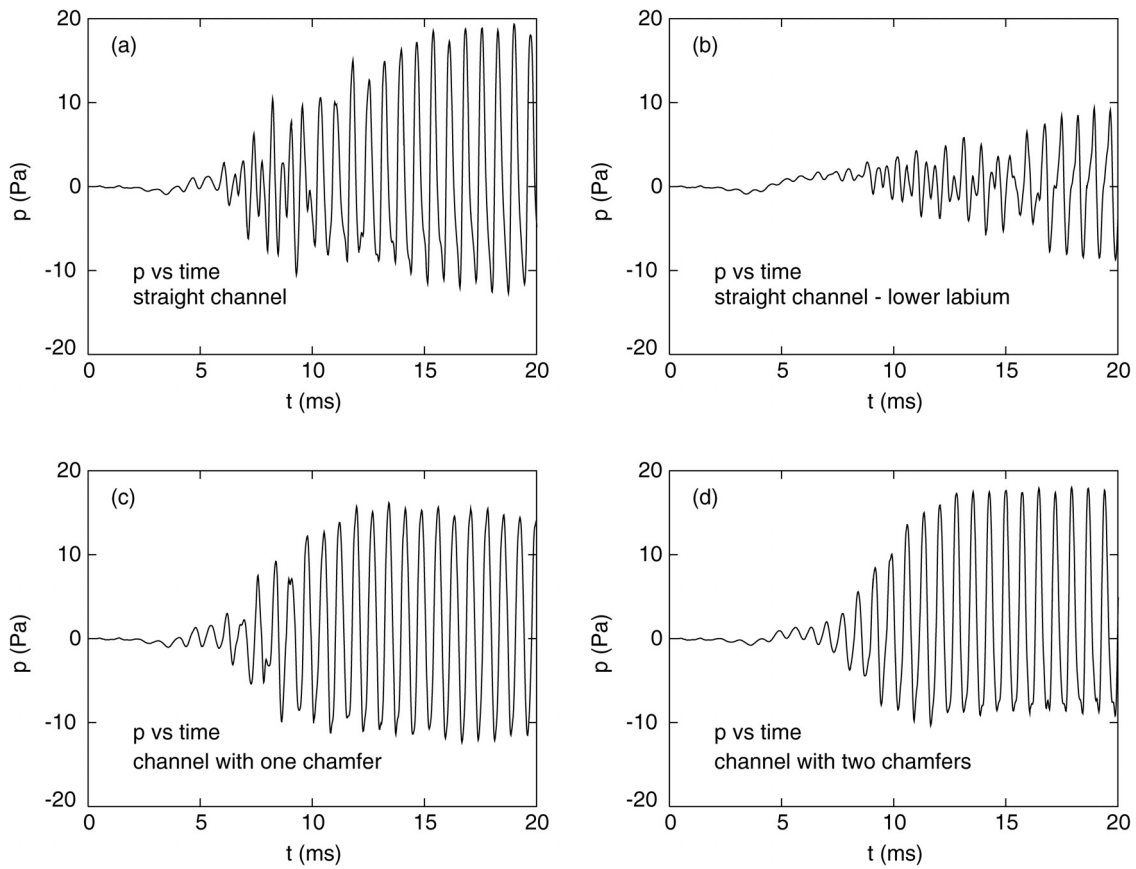

FIG. 5. Attack portion of the tone for several different labium and channel geometries. (a) Straight channel with the labium aligned with the center of the channel (an expanded view of the results in Fig. 4). (b) Straight channel with the labium aligned with the bottom of the channel. (c) Channel with a 45° chamfer on the bottom edge and a labium aligned with the center of the channel. (d) Channel with 45° chamfers on the bottom and top edges, and a labium aligned with the center of the channel. In all cases the blowing speed at the center of the channel was $u = 30$ m/s.

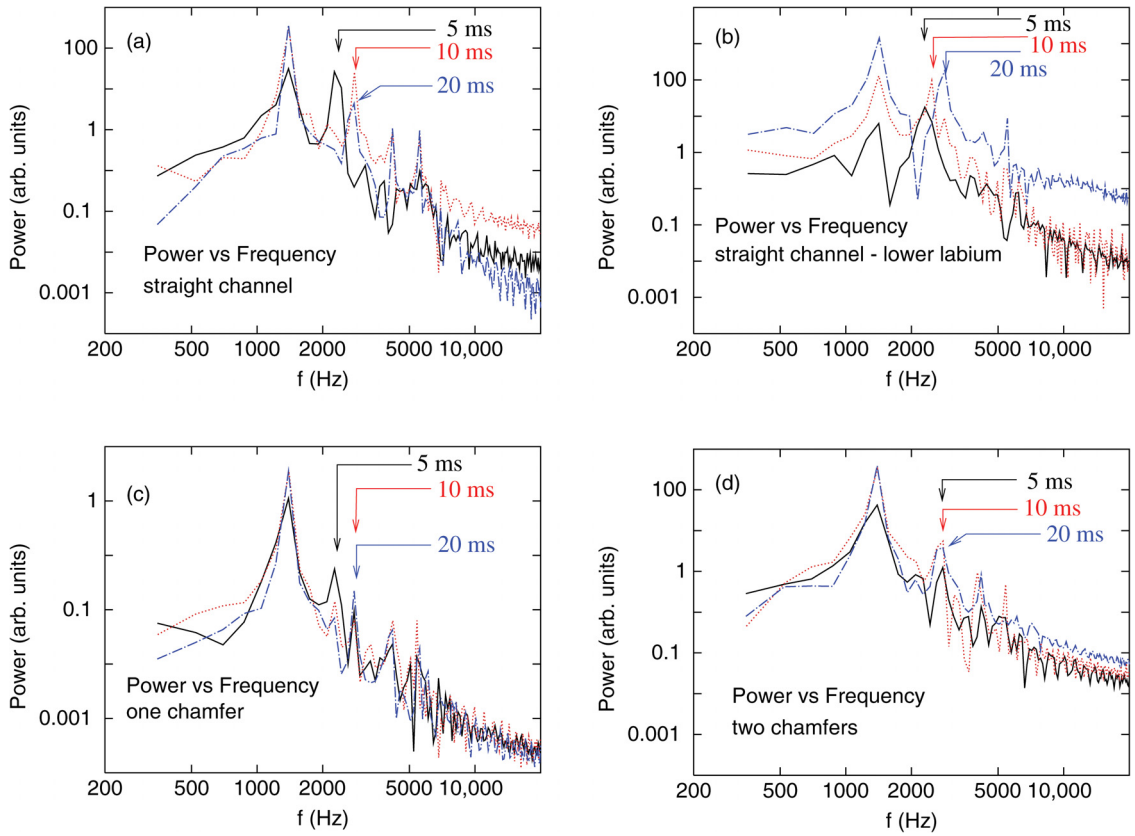

FIG. 6. (Color online) Spectra during the attack portions of the tone for the same labium and channel geometries described in the caption to Fig. 5. These spectra were calculated during the time periods 5–10, 10–15, and 20–25 ms as indicated in the figures. Note that the peaks are broadened due to the short transform times.

we plot values of the power derived from the two largest peaks in the spectra in Fig. 6 as functions of time, as obtained using short time Fourier transforms and summing the power in bins that contain the first and second peaks. These are referred to as peaks at f_1 (the fundamental) and f_2 (the second peak, which may be inharmonic). For the channel with two chamfers, the component at f_2 was always smaller than the fundamental component by at least an order of magnitude. This was not the case with the other channel and labium geometries, where the component at f_2 could be as large as or even larger than the fundamental component during the period between 5 and 10 ms. At long times, when the steady state was reached, the fundamental was always much stronger than the component at f_2, and the component at f_2 was always consistent with being a true harmonic ($f_2 = 2f_1$).

One of the main messages from the results in Figs. 6 and 7 is that straight channels exhibit much stronger harmonics during the attack transient. This conclusion was also reached by Segoufin *et al.*[27] from their experimental studies. However, they did not report quantitative results for the amplitudes of the harmonics in different cases, so a quantitative comparison with their results is not possible at this time. They also do not appear to have tested for the inharmonicities we find at early portions of the attack. We should also mention the work of Nolle and Finch[28] on the attack portion of the tones produced by flue organ pipes. They studied the effect of varying the rise time of the initial blowing pressure and found inharmonic components that were largest when this rise time was shortest. They observed significant inharmonicity when the rise time was between 1 and 10 periods of the fundamental oscillation; this is consistent with our findings for, e.g., the straight channel in Fig. 6. (Recall that in our modeling the rise time was about seven periods.) It is then interesting to note that a change in channel geometry for a recorder, such as the addition of chamfers, can greatly change or eliminate these inharmonicities. It would be interesting to see if a similar effect occurs with organ pipes.

B. Steady state spectrum

In all of the geometries considered in the previous subsection, the sound pressure as a function of time reached steady state (i.e., an oscillation with a constant amplitude and frequency composition) after about 25 ms. A typical spectrum showing the steady state spectrum for the sound pressure in Fig. 4 is given in Fig. 8; for this case, the channel was straight (no chamfers), and the labium was aligned with the middle of the channel. Here the blowing speed is squarely in the regime where the fundamental frequency of the tube dominates (see following text for a discussion at high blowing speeds). While the spectrum in Fig. 8 is dominated by the fundamental, components at the second, third, and higher harmonics are clearly visible. These harmonics appear to be true harmonics; to within the uncertainties, the frequency of the the peak labeled f_2 is twice the frequency of the fundamental, etc., for the third harmonic.

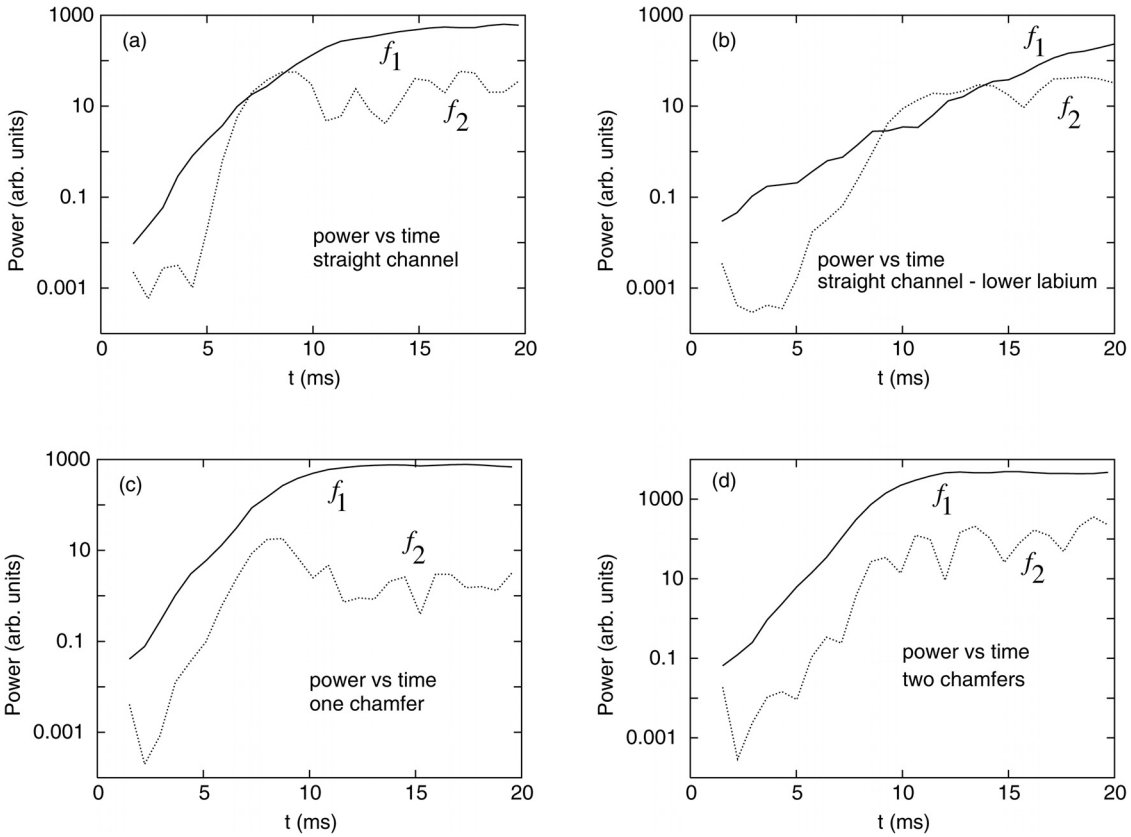

FIG. 7. Time dependence of the spectral components at f_1 (the fundamental, solid curves) and f_2 (dotted curves) during the attack portion of the tone for the different labium and channel geometries described in Figs. 5 and 6.

Figure 9 shows results for the power of the various harmonics for the different channel and labium geometries in Fig. 6. Here we have normalized the power of *all* of the components by the power of the fundamental (first harmonic) for the case of the straight channel (Fig. 8). The strengths of the fundamental components differ by as much as a factor of 2, and the second and third harmonics vary by an order of magnitude or more. This suggests that the tone color will be very different for the different geometries.

We can also compare these results to the experimental findings of Segoufin *et al.*[27] For the case of a straight channel, they found that the second and third harmonics were stronger (each by about a factor of 2 or 3) relative to the fundamental than we find for this geometry in Fig. 9. However, we caution that this comparison relies on obtaining the same value of the Strouhal number, which is difficult to guarantee. If we instead compare results at similar values of the blowing speed based on the transition to the second harmonic (i.e., overblowing), the agreement with the results of Segoufin *et al.* is somewhat better. This is an issue that will need further study.

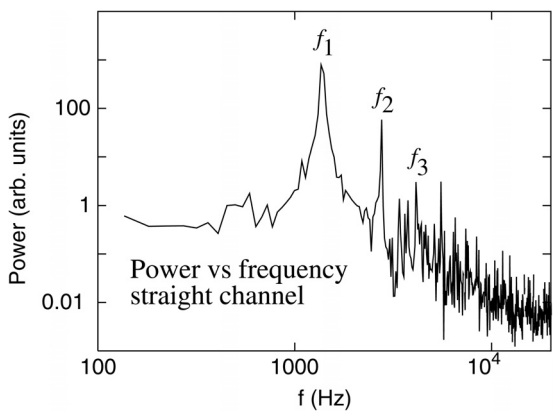

FIG. 8. Steady state pectrum of the recorder with a straight channel with the labium aligned with the center of the channel. The peaks associated with the fundamental, second harmonic, and third harmonic are labeled f_1, f_2 and f_3, respectively. The blowing speed at the center of the channel was $u = 30\,\mathrm{m/s}$.

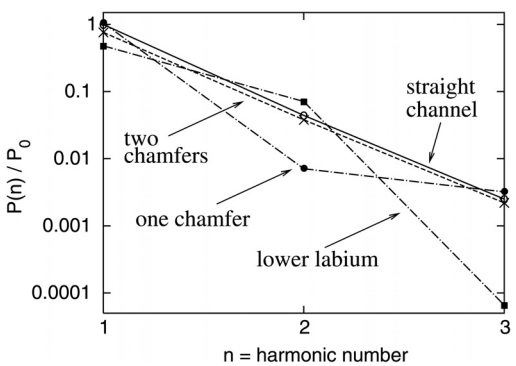

FIG. 9. Steady state power of the first three harmonics for various channel and labium geometries, all normalized by the power P_0 of the first harmonic for the case of a straight channel with the labium aligned with the center of the channel. For all cases $u = 30\,\mathrm{m/s}$ in the center of the channel.

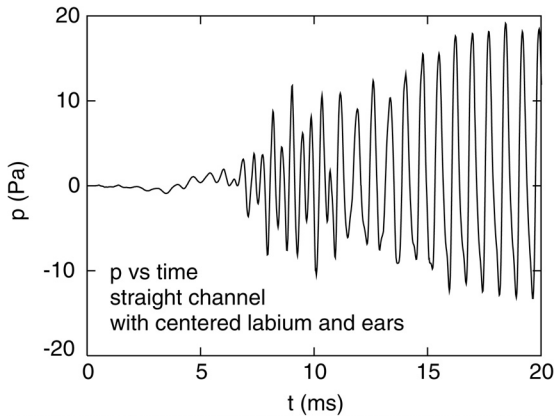

FIG. 10. Sound pressure as a function of time during the attack portion of the tone for a flue pipe with ears.

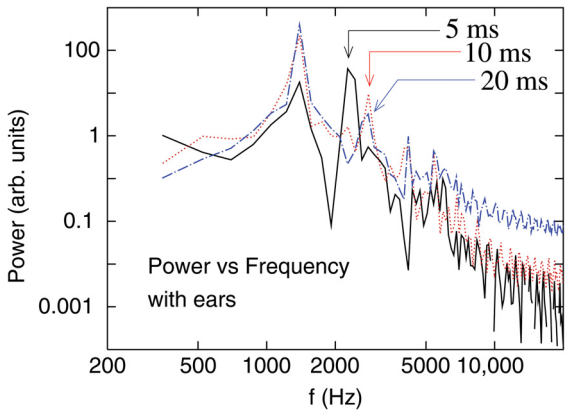

FIG. 11. (Color online) Spectrum at early times for a flue pipe with ears computed in the same way as the spectra in Fig. 6.

V. THE EFFECT OF EARS ON THE TONE OF A HYPOTHETICAL ORGAN PIPE

All of our discussion to this point has concerned channel and labium geometries that might be found in a recorder. An interesting geometry that is common in organ pipes (but not recorders) involves the addition of "ears" to the sides of the flue opening. These are flat plates placed on the sides of the opening and extending well above the top of the channel. Figures 10 and 11 show the behavior of the attack portion of the tone when ears are added to a recorder with a straight channel and labium aligned with the center of the channel. The ears of this hypothetical organ pipe extended 5.0 mm above the top edge of the labium (along the y direction) in Fig. 1(a) and were 12.0 mm long along the x direction, extending 4.0 mm to either side of the flue opening. This ear geometry was not taken from any particular organ pipe (and they may be a bit larger than commonly found in real organs). Our goal here was simply to understand the kinds of effects they can have on the behavior.

Here again we see at early times (5–10 ms) a strong peak near the frequency of the second harmonic, with a frequency f_2 distinctly below $2 \times f_1$. Comparing with the result for a straight channel without ears [Fig. 6(a)], we find that the ears strengthen the power at f_2 so that at early times this component is stronger than the fundamental component. The ears also affect the fundamental frequency of the steady state tone, shifting it to a slightly lower frequency, as expected because the presence of ears increases the effective length of the resonator at the end near the labium. In our case, we find a shift of about 20 Hz (approximately 1.5%). These results confirm that the effect of ears is sufficiently large to be of great use in tuning the instrument, both with regard to the pitch and to the nature of the attack.

Not surprisingly, the ears also affect the dynamics of the air jet. Figure 12 shows images of the jet at two separate times on two vertical planes that pass through the channel and flue opening. The top images show the air jet on the plane that passes through the middle of the channel while the bottom images show the air jet at the same times but on a

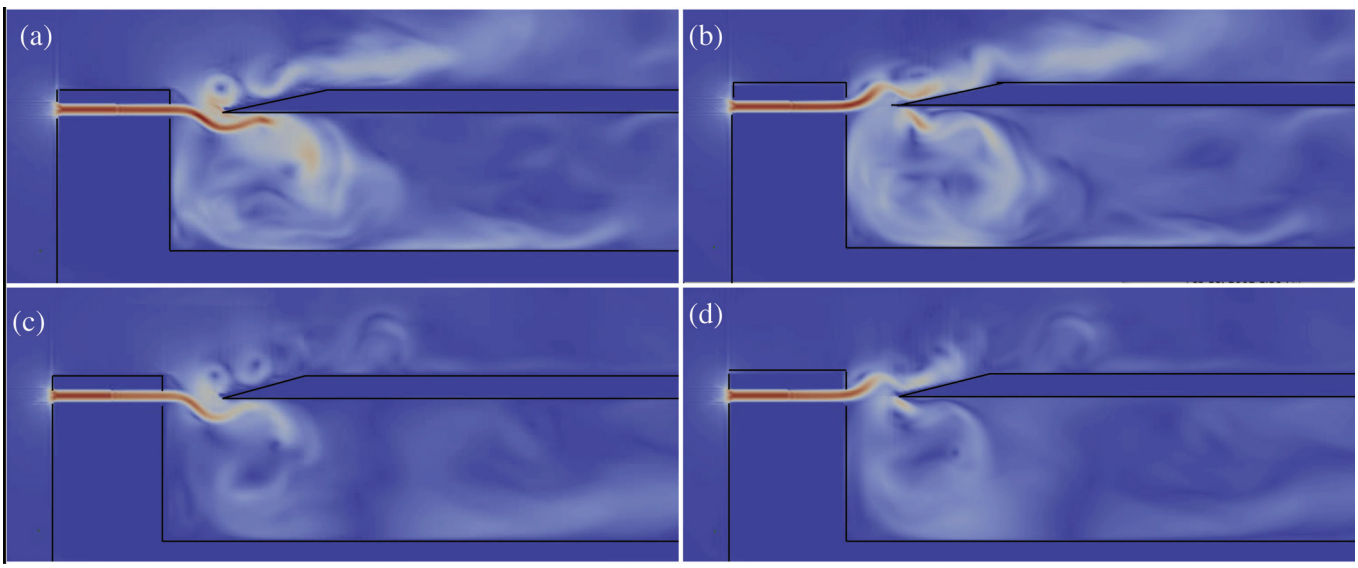

FIG. 12. Images of the air jet for a recorder with ears, all on an $x - y$ plane [Fig. 1(a)] that cuts through the recorder. (a) and (b) For the plane that passes through the center of the channel. (c) and (d) For a plane that passes just inside one of the side edges of the channel. Images (a) and (c) were recorded at the same time, and images (b) and (d) were recorded approximately half a period later. The blowing speed was $u = 30$ m/s.

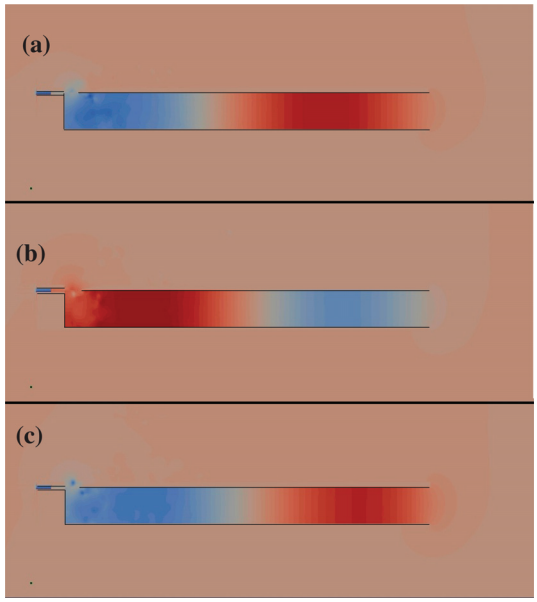

FIG. 13. Images of the density for a blowing speed of 45 m/s. Here the spectrum was dominated by the component at the frequency of the second harmonic f_2 although the first harmonic was not completely negligible (see following text). These images were obtained at times spaced by approximately half a period of the oscillation, $1/(2f_2)$.

plane that passes just inside a side edge of the channel and is thus very close to an ear. One would expect the presence of a nearby ear to somewhat dampen the motion of the jet due to the nonslip condition on the velocity at the surface of the ear, and that is precisely what is seen in Fig. 12. In the bottom images (obtained near an ear), the jet loses speed much sooner as it moves up and away from the channel, due to this damping. This effect is also visible but not quite as great for geometries without ears (as in Fig. 3) and will need to be taken into account in any detailed comparisons between experimental and numerical results for the jet shape and dynamics.

VI. EFFECTS AT HIGH BLOWING SPEEDS

All of the results shown in the preceding text were obtained at blowing speeds for which the recorder oscillated in its fundamental mode. As the blowing speed was increased, the harmonics increased in strength and eventually the second harmonic became largest.

Maps of the air density at a blowing speed for which oscillations at the second harmonic (with frequency f_2) were dominant are shown in Fig. 13. The image in (a) shows a standing wave with nodes near both ends of the resonator tube and at the center, giving a wavelength equal (apart from end corrections) to the length of the pipe, as expected for an oscillation at the second harmonic. The image in (b) was recorded approximately half a period [a time $1/(2f_2)$] later and the image in (c) was obtained a half period after that. Taken together the results in Fig. 13 show precisely the behavior expected for this mode.

Figure 14 shows a series of images of the speed of the air jet for the same conditions. These images span approximately one period of an oscillation at the fundamental frequency f_1. From these images, one can see the periodicity at the frequencies of both the fundamental and the second harmonic. For example, images (b) and (f), which differ in time by $1/f_2$, both show the air jet extending upward above the labium, but the detailed spatial variation of jet speed is distinctly different in the two cases. This can be explained by

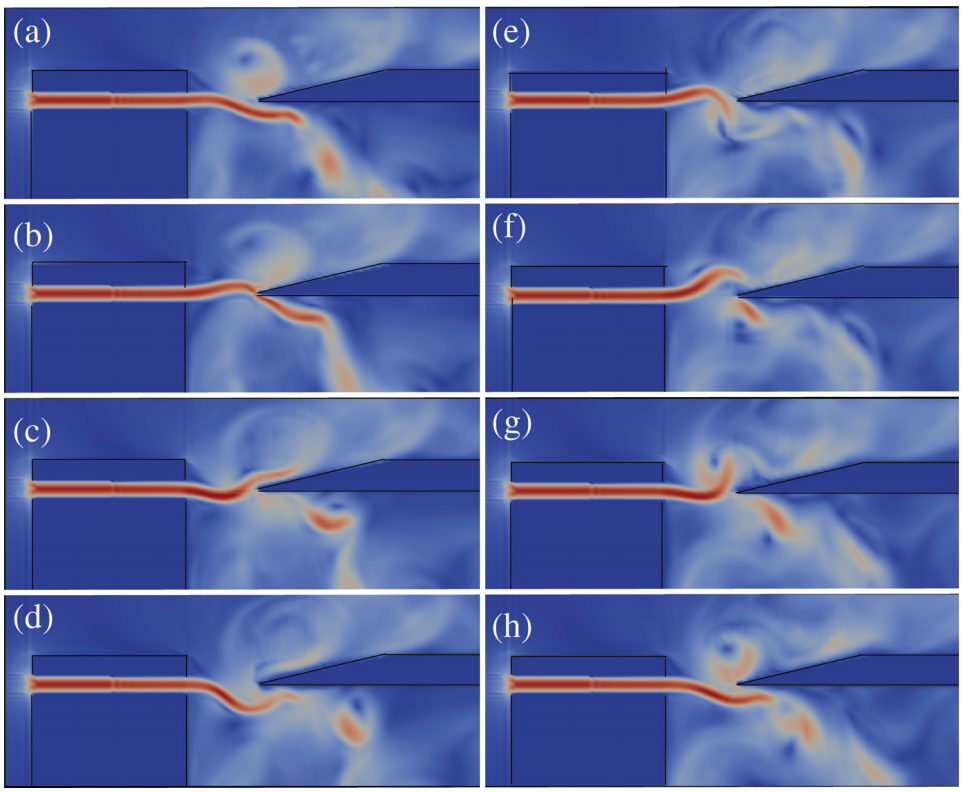

FIG. 14. Images of the air jet for a blowing speed of 45 m/s for which the oscillation at the second harmonic is dominant. These images span approximately one period of the fundamental frequency of oscillation.

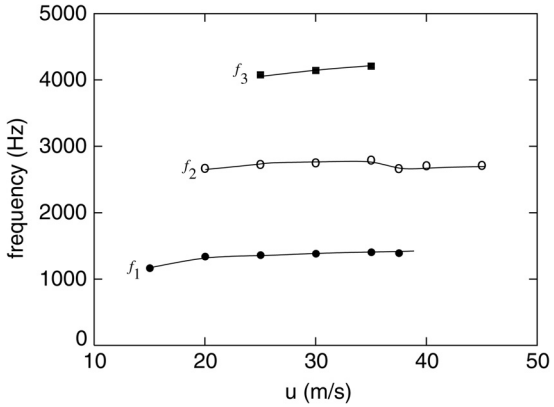

FIG. 15. Frequencies of the three lowest spectral components during the steady state portion of the tone as a function of blowing speed u in the center of the channel. The labels indicate the fundamental frequency f_1 and its harmonics f_2 and f_3.

an oscillation with two spectral components with frequencies that differ by a factor of two.

Some parameters associated with the spectra for different blowing speeds are shown in Figs. 15 and 16. There is a clear transition to a mode dominated by the second harmonic of the resonator tube. This transition occurs near $u = 37$ m/s, as can be seen from Fig. 16. As u is increased through that transition, the frequency of the second harmonic drops a small but noticeable amount, and the frequency of the fundamental also decreases slightly (this decrease is barely visible in Fig. 15). Above that blowing speed, the component at the third harmonic becomes negligibly small. This transition has been observed in many experiments (and by many recorder players) and is often studied by observing how the frequency varies as the blowing speed is gradually increased or decreased. Such experiments generally show hysteresis; that is, a range of blowing speeds for which the frequency can assume two different values, depending on how the blowing speed is varied. As we have performed our modeling, we are not able to study this hysteresis; in our simulations, we have always started each simulation with a blowing speed of zero, which is then ramped quickly (in 5 ms) to a final value. Comparisons of the results in Figs. 15 and 16 with

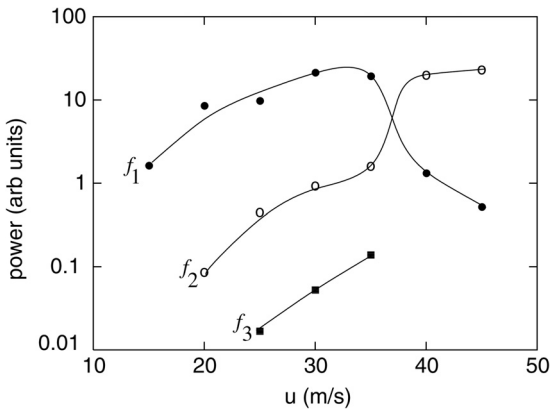

FIG. 16. Power of the three lowest harmonics during the steady state portion of the tone as a function of blowing speed u in the center of the channel.

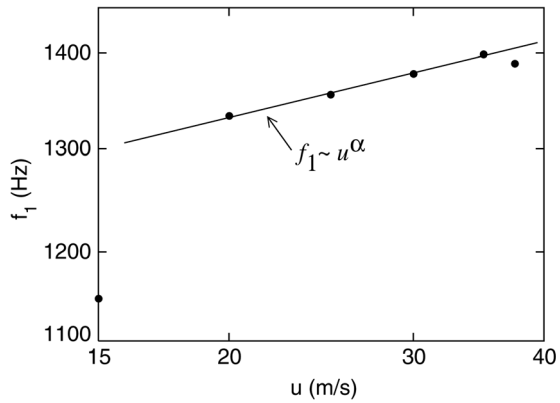

FIG. 17. Frequency of the oscillation frequency as a function of blowing speed u. On this log-log plot a straight line indicates a power law variation of f_1 with u.

experiments must take account of this difference between the experiments and our modeling.

Figure 17 shows the behavior of f_1 on an expanded scale. The results suggest that there are three different regimes. (1) A region at low u, below about 20 m/s, where the behavior is either dominated by or heavily influenced by the edge tone. This was shown nicely by the results of Ref. 14 in two dimensions. In this regime, Miyamoto and coworkers showed that the frequency is approximately proportional to u as expected theoretically and thus falls rapidly as u is decreased. (2) A region at high u where the behavior is affected by the transition to the second harmonic. In Fig. 17 that region is above about $u = 35$ m/s. (3) An intermediate region where the variation of f_1 with u is much weaker. This is presumably the musically useful range.

Bak[29] reported a study of the variation of pitch with blowing speed for a number of different notes with a number of different recorders. He found behavior consistent with

$$f_1 \approx k u^{\alpha}, \tag{8}$$

and his results are all consistent with $\alpha \approx 0.05$. The straight line in Fig. 17 shows a power law dependence and is consistent with our results in region 3 defined in the preceding text. The straight line drawn in Fig. 17 corresponds to $\alpha \approx 0.085$, and even allowing for generous uncertainties this is a considerably higher exponent than the value found by Bak. The reason for this difference is not clear, but it may be due to the fact that our model recorder is much shorter than the recorders studied by Bak. We speculate that this may make the end corrections in our case more sensitive to u; this is an issue that needs further study.

VII. SUMMARY AND OUTLOOK

We have used a direct numerical solution of the Navier–Stokes equations to study the aeroacoustics of the recorder in three dimensions. We have shown how such simulations can yield qualitative information concerning the dynamics of the density and air jet, and quantitative results for the sound spectrum and how it depends on blowing speed. We have explored how the attack portion of the tone depends on the detailed geometry of the channel and labium

and found a significant inharmonic component at early stages of the attack. We also find that the timbre of the steady state tone depends strongly on this geometry. It will be interesting to explore how this dependence on channel and labium geometry might be used to produce recorders with different tonal and playing properties.

One purpose of the present work was to demonstrate that the computational methods used here give an accurate description of the aeroacoustics of interest in a wind instrument. We believe that our results do indeed confirm this point and set the stage for applying these methods to study other aspects of flue instruments and of other wind instruments in general. Full musical tones that could be used in listening tests should be feasible soon.

ACKNOWLEDGMENT

I thank the Rosen Center for Advanced Computing at Purdue University for access to the computational resources essential for this work.

[1]N. Giordano, "Direct numerical simulation of a recorder," J. Acoust. Soc. Am. **133**, 1113–1118 (2013).
[2]P. A. Skordos, "Modeling of flue pipes: Subsonic flow, lattice Boltzmann and parallel distributed distributed computers," Ph.D. thesis, MIT, Cambridge, MA, 1995.
[3]P. A. Skordos and G. J. Sussman, "Comparison between subsonic flow simulation and physical measurements of flue pipes," in *Proceedings of the International Symposium on Musical Acoustics*, Dourdan, France (1995), pp. 1–6.
[4]H. Kühnelt, "Simulating the mechanism of sound generation in flutes using the lattice Boltzmann method," in *Proceedings of the Stockholm Music Acoustics Conference (SMAC 03)*, SMAC1–SMAC4 (2003).
[5]H. Kühnelt, "Simulating the mechanism of sound generation in flutes and flue pipes with the lattice-Boltzmann-method," in *Proceedings of the International Symposium on Musical Acoustics*, Nara, Japan (2004), pp. 251–254.
[6]H. Kühnelt, "Vortex sound in recorder- and flute-like instruments: Numerical simulation and analysis," in *Proceedings of the International Symposium on Musical Acoustics*, Barcelona, Spain (2007), pp. 1–8.
[7]A. R. da Silva and G. Scavone, "Coupling lattice Boltzmann models to digital waveguides for wind instrument simulations," in *Proceedings of the International Symposium on Musical Acoustics*, Barcelona, Spain (2007), pp. 1–7.
[8]A. R. D. Silva, H. Kühnelt, and G. Scavone, "A brief survey of the lattice-Boltzmann method," in *Proceedings of the International Congress on Acoustics*, Madrid, Spain (2007), pp. 1–6.
[9]Y. Obikane and K. Kuwahara, "Direct simulation for acoustic near fields using the compressible Navier–Stokes equation," in *Computational Fluid Dynamics 2008* (Springer, New York, 2009). pp. 85–91.
[10]Y. Obikane, "Direct simulation on a fipple flute using the compressible Navier–Stokes equation," World Acad. Sci. Eng. Technol. **4**, 794–798 (2009).
[11]Y. Obikane, "Computational aeroacoustics on a small flute using a direct simulation," in *Computational Fluid Dynamics 2010*, edited by A. Kuzmin (Springer-Verlag, New York, 2010), pp. 435–441.
[12]M. Miyamoto, Y. Ito, K. Takahashi, T. Takami, T. Kobayashi, A. Nishida, and M. Aoyagi, "Applicability of compressible LES to reproduction of sound vibration of an air-reed instrument," in *Proceedings of the International Symposium on Musical Acoustics*, Sydney and Katoomba, Australia (2010).
[13]M. Miyamoto, Y. Ito, K. Takahashi, T. Takami, T. Kobayashi, A. Nishida, and M. Aoyagi, "Numerical study on sound vibration of an air-reed instrument with compressible LES," arXiv:1005.3413v1.
[14]M. Miyamoto, Y. Ito, T. Iwasaki, T. Akamura, K. Takahashi, T. Takami, T. Kobayashi, A. Nishida, and M. Aoyagi, "Numerical study on acoustic oscillations of 2d and 3d flue organ pipe like instruments with compressible LES," Acta Acust. Acust. **99**, 154–171 (2013).
[15]K. Takahashi, T. Iwasaki, T. Akamura, Y. Nagao, K. Nakano, T. Kobayashi, T. Takami, A. Nishida, and M. Aoyagi, "Effective techniques and crucial problems of numerical study on flue instruments," Proc. Meet. Acoust. **19**, 035021 (2013).
[16]N. Giordano, "Direct numerical simulation of the recorder in two and three dimensions," Proc. Meet. Acoust. **19**, 035062 (2013).
[17]N. Giordano, "Numerical modeling of a recorder in three dimensions," in *Proceedings of the Stockholm Music Acoustics Conference (SMAC 13)*, SMAC1–SMAC5 (2013).
[18]J. Martin, *The Acoustics of the Recorder* (Moeck, Berlin, 1993), 112 pp.
[19]J. J. D. Anderson, *Computational Fluid Dynamics* (McGraw-Hill, New York, 1995), 574 pp.
[20]R. W. MacCormack, "The effect of viscosity in hypervelocity impact cratering," AAIA Paper **69–354**, 1–7 (1969).
[21]A. Jameson, W. Schmidt, and E. Turkel, "Numerical solution of the Euler equations by finite volume methods using Runge Kutta time stepping schemes," AAIA Paper **81–1289**, 1–14 (1981).
[22]D. Botteldooren, "Acoustical finite-difference time-domain simulation in a quasi-Cartesian grid," J. Acoust. Soc. Am. **95**, 2313–2319 (1994).
[23]D. Botteldooren, "Finite-difference time-domain simulation of low-frequency room acoustic problems," J. Acoust. Soc. Am. **98**, 3302–3308 (1995).
[24]L. L. Beranek, "Acoustic impedance of commercial materials and the performance of rectangular rooms with one treated surface," J. Acoust. Soc. Am. **12**, 14–23 (1940).
[25]B. Fabre, A. Hirschberg, and A. P. J. Wijnands, "Vortex shedding in steady oscillation of a flue organ pipe," Acta Acust. Acust. **82**, 863–877 (1996).
[26]G. K. Batchelor, "Computation of the energy spectrum in homogeneous two-dimensional turbulence," Phys. Fluids Suppl. **12**, II-233–239 (1969).
[27]C. Ségoufin, B. Fabre, M. P. Verge, A. Hirschberg, and A. P. J. Wijnands, "Experimental study of the influence of the mouth geometry on sound production in a recorder-like instrument: Windway length and chamfers," Acta Acust. Acust. **86**, 649–661 (2000).
[28]A. W. Nolle and T. L. Finch, "Starting transients of flue organ pipes in relation to pressure rise time," J. Acoust. Soc. Am. **91**, 2190–2202 (1992).
[29]N. Bak, "Pitch, temperature and blowing pressure in recorder playing. study of treble recorders," Acustica **22**, 296–299 (1969).